

K.V. Korytchenko, V.F. Bolyukh, S.G. Buriakovskiy, Y.V. Kashansky, O.I. Kocherga

Electromechanical and thermophysical processes in the pulse induction accelerator of plasma formation

Introduction. Work on the creation and throwing of plasma formations is carried out in the world's leading scientific centers in various ways. The creation of a plasma formation with duration of several milliseconds and its acceleration in an open atmospheric environment to a distance of 0.5-0.6 m was achieved. To create plasma, the energy of the primary discharge circuit is used, followed by the acceleration of the gas-plasma formation with the help of the energy of the secondary circuit. Plasma formation is also obtained due to the electric explosion of a conductor in a rapidly decreasing strong magnetic field, etc. The **purpose** of the article is a theoretical and experimental study of electromechanical and thermophysical processes in a pulse induction accelerator, which ensures the creation of plasma formation due to thermal ionization as a result of the electric explosion of the conductor and its throwing in the atmospheric environment relative to the inductor. **Method.** For the analysis of electromechanical and thermophysical processes in the pulse induction accelerator of plasma formation (PIAPF), a mathematical model of the accelerator was developed and implemented in the Comsol Multiphysics software package, in which the armature does not change its shape and aggregate state during operation and takes into account the parameters of the accelerator distributed in space. **Results.** Calculated electromechanical and thermal characteristics of the accelerator. It is shown that the temperature rise in the aluminum foil armature is significantly nonuniform. The maximum temperature value occurs in the middle part of the foil closer to the outer edge, and this temperature is significantly higher than the boiling point of aluminum. **Scientific novelty.** Experimental studies of the PIAPF were carried out, in which the armature is made of aluminum and copper foil, and the inductor connected to the high-voltage capacitive energy storage device is made in the form of a flat disk spiral. It was established that during the operation of the PIAPF, the armature goes into a plasma state and moves vertically upwards, turning into a volumetric wad or a pile of small particles that rose to a considerable height relative to the inductor. Experimentally, the characteristic circular circuit of thermal heating of the copper foil of the armature, which is fixed on a glass-textolite sheet, is shown, which indicates a similar nature of plasma formation. **Practical value.** The results of experimental studies with an accuracy of up to 15 % coincide with the calculated ones and show the validity of the PIAPF concept, in which, due to the high density of the induced current in the armature, thermal ionization occurs as a result of an electric explosion of the conductor with its transition to the plasma state. And the interaction of the plasma formation with the magnetic field of the inductor leads to the appearance of an electrodynamic force that ensures its movement in the open atmospheric environment. References 17, figures 9.

Key words: pulse induction accelerator of plasma formation, mathematical model, electromechanical and thermal processes, experimental studies.

Вступ. Роботи по створенню та метанню плазмових утворень різними способами ведуться в провідних наукових центрах світу. Досягнуто формування плазмового утворення тривалістю декілька мілісекунд та його метання у відкритому атмосферному середовищі на відстань 0,5-0,6 м. Для створення плазми використовують енергію первинного розрядного кола з подальшим прискоренням газоплазмового утворення за допомогою енергії вторинного кола. Плазмове утворення отримують і за рахунок електричного вибуху провідника. **Метою** статті є теоретичне та експериментальне дослідження електромеханічних та теплофізичних процесів в імпульсному індукційному прискорювачі, який забезпечує формування плазмового утворення за рахунок термічної іонізації в результаті електричного вибуху провідника та метання його у атмосферному середовищі відносно індуктора. **Методика.** Для аналізу електромеханічних та теплофізичних процесів в імпульсному індукційному прискорювачі плазмового утворення (ППП) розроблена і реалізована в програмному пакеті Comsol Multiphysics математична модель прискорювача, в якій яркір не змінює своєї форми і агрегатного стану в процесі роботи та враховує розподілені у просторі параметри. **Результати.** Розраховані електромеханічні і теплові характеристики прискорювача. Показано, що перевищення температури в якорі, що виконаний у вигляді алюмінієвої фольги, суттєво нерівномірно. Максимальне значення температури має місце в середній частині фольги ближче до зовнішнього краю, причому ця температура значно перевищує температуру кипіння алюмінію. **Наукова новизна.** Проведені експериментальні дослідження ППП, у якого яркір виконаний з алюмінієвої та мідної фольги, а індуктор, що підключається до високовольтного ємнісного накопичувача енергії, виконаний у вигляді плоскої дискової спіралі. В процесі роботи ППП яркір переходить в плазмовий стан і переміщується вертикально вгору, перетворюючись в об'ємний комок, або на скупчення маленьких частинок, які здіймалися на декілька метрів відносно індуктора. Експериментально показано характерний круговий контур термічного нагрівання мідної фольги якоря, яка закріплена на листі склотекстоліту. **Практична цінність.** Результати експериментальних досліджень з точністю до 15 % співпадають з розрахунковими і показують справедливості концепції ППП, в якому за рахунок високої густини індукваного струму в якорі відбувається термічна іонізація в результаті електричного вибуху провідника з переходом його в плазмовий стан. Взаємодія плазмового утворення з магнітним полем індуктора призводить до появи електродинамічної сили, яка забезпечує його переміщення у відкритому атмосферному середовищі на декілька метрів. Бібл. 17, рис. 9.

Ключові слова: імпульсний індукційний прискорювач плазмового утворення, математична модель, електромеханічні та теплові процеси, експериментальні дослідження.

Introduction. Plasma technologies are used in various structural and technological systems and devices, in scientific research, etc. One of the directions of such

research is the formation of plasma formations and throwing them at a certain distance from the source of formation. Such work is carried out in the leading

scientific centers of the world, primarily in the USA: Princeton Laboratory of Plasma Physics, Los Alamos National Laboratory, University of New Hampshire, Swarthmore Laboratory of Magnetodynamics, etc. [1-4]. The University of Missouri, USA is investigating the acceleration of plasma formation in an open atmospheric environment [5]. The duration of existence of a plasma formation is a few milliseconds, and it moves in the air for a small distance of 0.5-0.6 m.

For the formation of plasma, the energy of the primary discharge circuit is used [6]. The formation of plasma in the form of a ring occurs due to the gas-dynamic process of turbulation of the gas-plasma jet. Acceleration of gas-plasma formation is carried out using the energy of the secondary circuit. The output of thermal plasma from the forechamber is provided by gas-dynamic, not electrodynamic forces.

Plasma formation is also formed due to the electrical explosion of a conductor in a rapidly decreasing magnetic field [7]. The magnetic field is formed due to the current flowing through the plasma, which is formed in the form of a spiral in the wake of the explosion of the conductor. To create conditions for the stability of the ring due to the energy of the magnetic field, it is assumed that the process of returning the energy of the magnetic field to the electric energy of the capacitor charge is interrupted.

In induction plasmotrons, for the formation of a plasma ring, the method of inducing a discharge in a low-pressure gas environment with subsequent increase to atmospheric pressure, or plasma formation in the area near the inductor due to an arc discharge is used [8-10]. Plasmotrons provide induction of eddy current in the plasma formation in atmospheric conditions, but do not solve the problem of magnetic field energy accumulation in the plasma formation.

Analysis of accelerators of plasma formations. A known pulse plasma accelerator is containing electrodes, one of which is made in the form of a copper rod, and the other in the form of a plate. Ablation occurs under the action of an electric discharge between the electrodes in a solid dielectric substance [11]. The accelerator operates under low gas pressure in the accelerator channel. A pulse plasma accelerator is also known, which contains an accelerating channel formed by two electrodes with a Teflon insulator located between them, which is the working substance [12].

These accelerators have low efficiency and specific power, due to the use of only the energy stored by the electric field for acceleration. The effectiveness of these accelerators is limited by the long process of creating the working substance due to the limited speed and nonuniformity of its evaporation.

There is a well-known plasma accelerator, which contains electrodes connected through an ohmic and inductive load to a capacitive energy storage (CES), an end ceramic insulator that separates the electrodes and dielectric checkers installed between the electrodes, made of the material in which the ablation takes place [13]. When a high-voltage pulse is applied to the electrodes, as a result of a surface breakdown, a plasma formation is

formed, which short-circuits the electrodes of the accelerator. The working substance that evaporates from the surface of the dielectric checkers is ionized and accelerated under the influence of electromagnetic forces and gas-dynamic pressure. In this accelerator, the efficiency of acceleration is increased due to the use of both electromagnetic forces and gas-dynamic pressure. However, it has a low specific power due to the use of only electrical energy to create electromagnetic and gas-dynamic forces.

There is a known plasma accelerator consists of a cylindrical guide tube, an external hollow cylindrical magnet and a system of thermal ionization of matter to the plasma state [14]. One end of the pipe is in the air environment, and on the other end there is a gas flow formation system using a gas turbine engine. The system of thermal ionization of matter consists of discharge electrodes located inside the guide tube and an induction plasma heater. The electromagnetic coil of the heater, which covers the guide tube, ensures the formation of plasma inside the guide tube. Due to the gas turbine engine, a heated gas flow is formed, which is directed into the cylindrical pipe. Gas heated above 1000 °C is sent to the thermal ionization system, where it is heated by arc discharges to a high temperature (5000-10000 °C). The gas enters the region of the induction heater, where a ring-shaped plasma is formed. Under the action of pulse magnetic fields alternately created by magnets located along the cylindrical guide tube, plasma formation is accelerated.

This device achieves a high specific power due to the combined use of the chemical energy of fuel combustion and the energy of the electromagnetic field. But the well-known accelerator has a too complicated design.

An inductive accelerator is known, which ensures the creation and acceleration of plasma in an air environment [15]. The accelerator consists of a coaxially installed fixed disk inductor excited by CES, and a working substance located opposite the inductor, which during thermal ionization due to the induced current passes into a plasma state with further acceleration along the coaxial axis under the action of electrodynamic forces. This accelerator has a simple design, but the plasma in the form of a ring cannot move a long distance relative to the inductor. Radially directed electrodynamic forces arise in the plasma ring, which «tear» the ring, and thus interrupt the flow path of the induced current.

Thus, the task of creating an accelerator of plasma formation, which ensures its movement in the air medium for a considerable distance, is urgent.

The goal of the article is a theoretical and experimental study of electromechanical and thermophysical processes in a pulse induction accelerator, which ensures the formation of a plasma formation due to thermal ionization as a result of an electric explosion of a conductor and throwing it in the atmospheric environment relative to the inductor.

Mathematical model of the accelerator. The difficulties of calculating the pulse inductive accelerator

of plasma formation (PIAPF) are primarily caused by the uncertainty of the plasma formation parameters, which change dynamically. To determine the general characteristics of electromechanical and thermal processes, we will assume that the armature is made solid and does not change its shape and aggregate state during the operation of the accelerator. To implement a mathematical model with spatially distributed parameters, we will use a system of partial differential equations with respect to spatial and temporal variables [16].

The mathematical model of electromagnetic processes in PIAPF, which includes a fixed inductor and a moving conductive armature, is presented in a cylindrical coordinate system in terms of a magnetic vector potential \vec{A}_i , which has a φ component.

The differential equations with respect to the φ component of the magnetic vector potential in the region of the inductor Ω_1 give the form:

$$\gamma_1 \frac{\partial A_{1\varphi}}{\partial t} + \frac{1}{\mu_0} \frac{\partial^2 A_{1\varphi}}{\partial z^2} + \frac{1}{\mu_0} \frac{\partial}{\partial r} \left(\frac{1}{r} \cdot \frac{\partial(rA_{1\varphi})}{\partial r} \right) = - \frac{i_1(t) \cdot N_1}{S_1} k_{1s}, \quad (1)$$

in the region of solid conductive armature Ω_2 :

$$\gamma_2 \frac{\partial A_{2\varphi}}{\partial t} + \frac{1}{\mu_0} \frac{\partial^2 A_{2\varphi}}{\partial z^2} + \frac{1}{\mu_0} \frac{\partial}{\partial r} \left(\frac{1}{r} \cdot \frac{\partial(rA_{2\varphi})}{\partial r} \right) - v_{z2}(t) \cdot \frac{\gamma_2}{\mu_0} \cdot \frac{\partial A_{2\varphi}}{\partial z} = 0 \quad (2)$$

in the region of air environment Ω_0 :

$$\frac{1}{\mu_0} \frac{\partial^2 A_{0\varphi}}{\partial z^2} + \frac{1}{\mu_0} \frac{\partial}{\partial r} \left(\frac{1}{r} \cdot \frac{\partial(rA_{0\varphi})}{\partial r} \right) = 0, \quad (3)$$

where $j_1(t)$ is the tangential component of the current density in the inductor; $i_1(t)$ is the instantaneous value of the current in the inductor; γ_1 , γ_2 is the specific conductivity of the inductor and armature, respectively; μ_0 is the magnetic constant; $v_{z2}(t)$ is the speed of the armature; N_1 is the number of turns of the inductor; S_1 is the cross-sectional area of the inductor; k_{1s} is the inductor filling factor.

Differential equations (1) – (3) are supplemented by the corresponding boundary and initial conditions:

$$\begin{aligned} \frac{1}{\mu_0} \text{rot} A_1 \cdot n &= - \frac{1}{\mu_0} \text{rot} A_2 \cdot n; \\ \text{rot} A_1 \cdot n &= - \text{rot} A_2 \cdot n; \\ A_{1\varphi}(0) &= A_{2\varphi}(0) = 0, \end{aligned} \quad (4)$$

where A_i is the magnetic vector potential of the magnetic field of the i -th region; n is the unit normal vector.

The axial component of the force acting on the accelerator armature is determined using the corresponding component of the Maxwell tension tensor T :

$$f_z = \oint_S 2\pi T_z ds = \frac{1}{\mu_0} \oint_S 2\pi (B_r \cdot B_z) ds, \quad (5)$$

where B_r , B_z are the radial and axial component of the magnetic flux density.

The electrical state of the accelerator can be described by equations:

$$2\pi \frac{N_1}{S_1} \int_{S_1} \frac{dr A_{1\varphi}}{dt} dr dz + (L_0 + L_1) \frac{di_1}{dt} + i_1(R_0 + R_1) + u_C = 0, \quad (6)$$

$$2\pi \frac{1}{S_2} \int_{S_2} \frac{dr A_{2\varphi}}{dt} dr dz + L_2 \frac{di_2}{dt} + i_2 R_2 = 0, \quad (7)$$

where L_0 , R_0 are the inductance and active resistance of the excitation circuit, respectively; R_1 , R_2 are the active resistances of the inductor and armature, respectively; L_1 , L_2 are the inductances of the inductor and the armature, respectively; i_2 is the instantaneous value of the current in the armature; S_2 is the cross-sectional area of the armature; u_C is the CES voltage, which is supplemented by the appropriate initial conditions.

Thermal processes in the PIAPF are described using the equation:

$$\begin{aligned} c_k(T) \cdot \gamma_k \frac{\partial T_k}{\partial t} &= \\ &= \frac{\partial}{\partial r} (\lambda_k(T) \frac{\partial T_k}{\partial r}) + \frac{1}{r} \lambda_k(T) \frac{\partial T_k}{\partial r} + \frac{\partial}{\partial z} (\lambda_k(T) \frac{\partial T_k}{\partial z}) + \\ &+ j_k^2(t) \cdot \rho_k(T), \end{aligned} \quad (8)$$

where $c_k(T)$ is the average specific heat capacity of the k -th active element (inductor and armature); γ_k is the average material density of the k -th active element; $j_k(t)$ is the current density of the k -th active element; $\lambda_k(T)$ is the thermal conductivity of the k -th active element; $\rho_k(T)$ is the resistivity of the k -th active element; T_k is the temperature distribution in space and time of the k -th active element.

On the cooled surfaces of the active elements, the system of equations (8) is supplemented by boundary conditions of the third kind, which takes into account convective and radiative heat exchange, and on the axis of symmetry by boundary conditions of the second kind.

The mathematical model of the PIAPF with nonuniform distribution of currents in the inductor and armature is implemented in the *Comsol Multiphysics* software package using the Finite Element Method when taking into account all relationships between physical processes [17]. Here, data is exchanged between processes, calculation regions are allocated for each physical problem, provided that the mesh division is consistent for all problems. Modeling is performed in the following sequence:

- physics modules («Magnetic fields», «Electrical circuit», «Heat transfer in solid», «Fluid structure interaction») are selected, which implement the corresponding tasks, dimensions (2D), model type (time-dependent) and calculation methods;
- the geometry of the accelerator is formed and the calculation regions for the selected physical problems are determined;
- output data are set in the form of constant values and functions that describe the relationship between parameters, for example, the dependence of specific resistance on temperature;
- initial and boundary conditions of the considered physical problems are set;

- discretization of calculation regions is carried out taking into account the geometric model of the electrodynamic accelerator;

- methods of solving the considered problems MUMPS, PARDISO are chosen and numerical calculations are carried out.

The calculation area of the model was a cylinder with radius whose value was more than 5 times greater than the radius of the farthest element of the accelerator in the radial direction from the z axis. The height of the calculated cylinder was more than 10 times higher than the largest height of the accelerator elements. This made it possible to achieve the required accuracy with acceptable calculation time, considering the calculation boundary to be conditionally infinite.

The model used the «Free triangular» mesh with «Extra fine» element sizes (the maximum mesh element size for remote areas of the environment was 5 mm, and for the accelerator, the mesh element size was chosen in the interval from (0.001 to 1 mm)). Relative displacement of elements of the accelerator was determined by the use of Automatic remeshing (criterion $\text{mod1.fsi.minqual} > 0.2$). Spatial discretization consists in dividing a limited area into separate piecewise continuous subareas. The set of such elements is defined as a mesh or triangulation, which is a model of the calculation area. Moreover, for each of the physical modules («Magnetic fields», «Electrical circuit», «Heat transfer in solid»), the interpolation of the solution for individual finite elements, determined by quadratic or cubic discretization, was used. The main variables are approximated by nodal values multiplied by base vector that is required for interpolation within the element. An implicit finite-difference scheme of the fifth order is used for time approximation.

Electromechanical and thermal processes of the accelerator. Consider the PIAPF, in which the fixed inductor is made in the form of a flat spiral made of steel, and the armature is made in the form of a disk-shaped aluminum foil, located coaxially with respect to the inductor. PIAPF parameters are as follows: **CES:** voltage $U_0 = 25$ kV, capacity $C_0 = 360$ μF ; **inductor:** number of turns $N_1 = 7$, inner diameter $D_{in} = 10$ mm, outer diameter $D_{ex} = 600$ mm, cross-sectional area of the turn $S_1 = 5 \times 25 = 125$ mm^2 ; **armature:** thickness $h_2 = 8$ μm ; outer diameter $D_{ex} = 600$ mm, distance from the inductor $z_0 = 0.5$ mm; **excitation circuit:** $L_0 = 1.5$ μH , $R_0 = 50$ $\text{m}\Omega$.

Figure 1 presents the calculated characteristics of the PIAPF, namely, the change in the CES voltage u_C , the current density in the inductor j_1 and in the armature j_2 (a), the current density in the armature distributed along its radius at the moment of maximum current (b).

There is a non-simultaneous increase in the maximum values of the currents in the inductor and the armature. The armature current reaches its maximum value after about 0.15 ms, while the inductor current reaches its maximum value after about 0.75 ms. Moreover, the density of the induced current in the armature is nonuniform across the cross-section in the radial direction: in the middle part, closer to the outer edge, it reaches a maximum value of $j_2 = 118$ kA/mm^2 , and on the outer edge it decreases to $j_2 = 76$ kA/mm^2 .

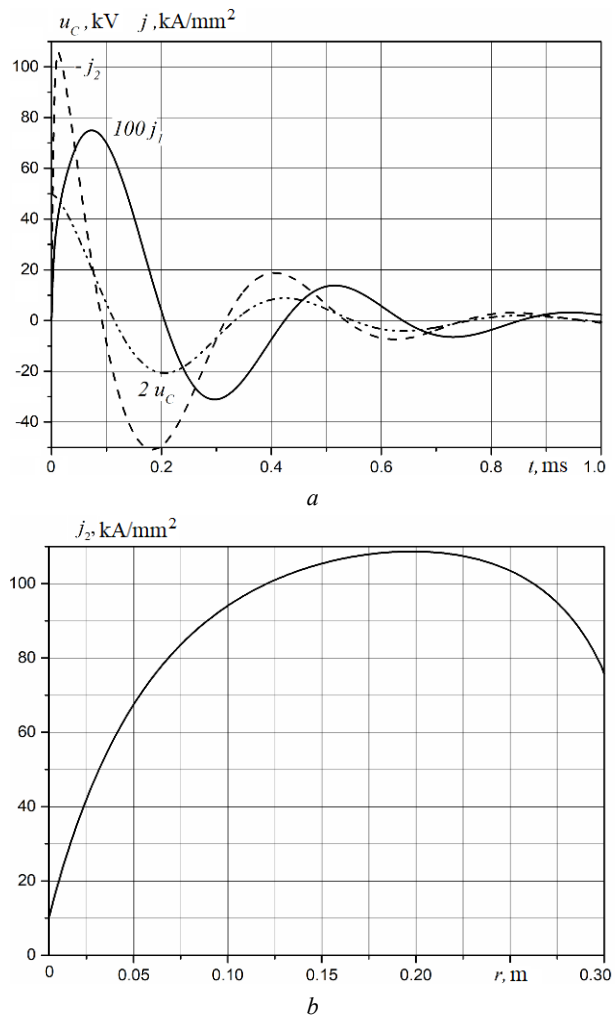


Fig. 1. Calculated characteristics of the PIAPF: a – change in the CES voltage and current density in the inductor and armature; b – current density distribution in the armature at the moment of maximum induced current

Figure 2 shows the electrodynamic force f_{z2} , the speed v_z and the displacement h_z of the armature. The maximum value of the electrodynamic force of repulsion reaches about $f_{z2} = 185$ kN. But due to the phase shift between the currents in the inductor and the armature in the interval of 0.9 – 2.1 ms, the electrodynamic force of attraction acts on the armature, which is much smaller than the force of repulsion. As a result of this nature of the force, the speed of the armature reaches a maximum value of approx. $v_z = 113$ m/s at 0.08 ms, after which the speed decreases to 66 m/s at 0.2 ms after the start of the work process with a slight increase later.

Figure 3 shows the change and radial distribution at the moment of the maximum current of exceeding the temperature of the armature θ_2 . The change in θ_2 over time is determined by the nature of the change in the current density in the armature j_2 . The temperature rise increases to a value of about $\theta_2 = 4200$ $^\circ\text{C}$ at the moment of 0.6 ms from the start of the work process. After that, there is a slight decrease to $\theta_2 = 4000$ $^\circ\text{C}$ with a gradual increase to $\theta_2 = 6300$ $^\circ\text{C}$ and higher after 0.25 ms.

But the temperature excess is distributed over the cross-section of the armature (aluminum foil) in the radial direction significantly nonuniformly. In the center of the

foil $\theta_2 = 0$. The maximum value of $\theta_2 = 7900$ °C occurs in the middle part of the armature closer to the outer edge. Note that the boiling point of aluminum is 2519 °C, and that of copper is 2580 °C.

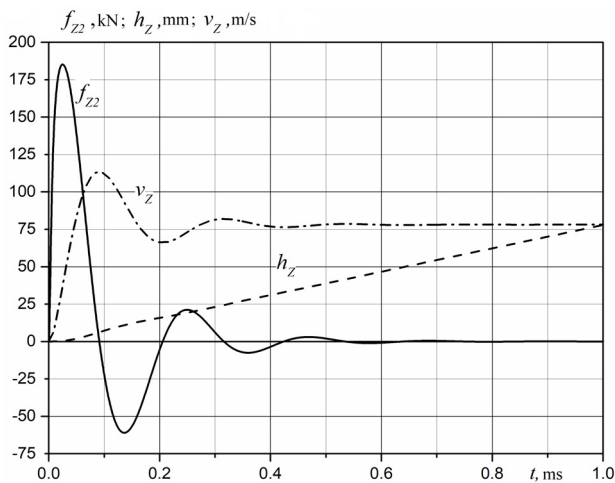


Fig. 2. Electrodynamic force f_{zz} , speed v_z and displacement h_z of the armature in PIAPF

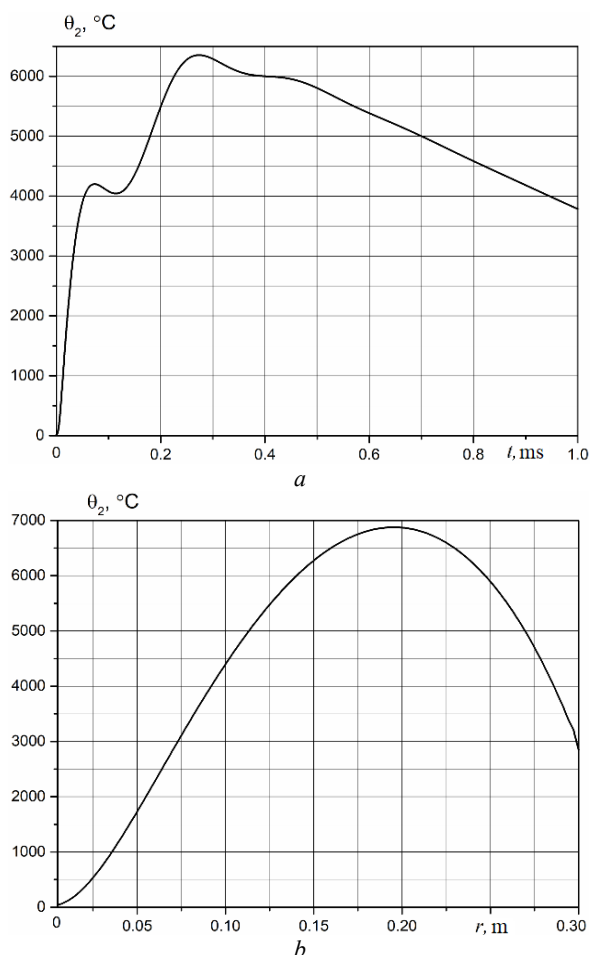


Fig. 3. Armature temperature rise: change in temperature rise over time (a), radial distribution of temperature rise at the moment of maximum current (b)

In order to validate the mathematical and computer models, the energy balance of the PIAPF was checked. Figure 4 presents: W_C – CES energy; W_{floss} – heat losses in the armature; W_i – heat losses in the inductor; W_{mag} – magnetic field energy; W_{Sr} – heat losses on the limiting

resistor and lead wires; W_{Sind} – magnetic energy on underwater wires; W_{kin} – kinetic energy. Since the energy balance is fulfilled, this indicates the reliability of the obtained results.

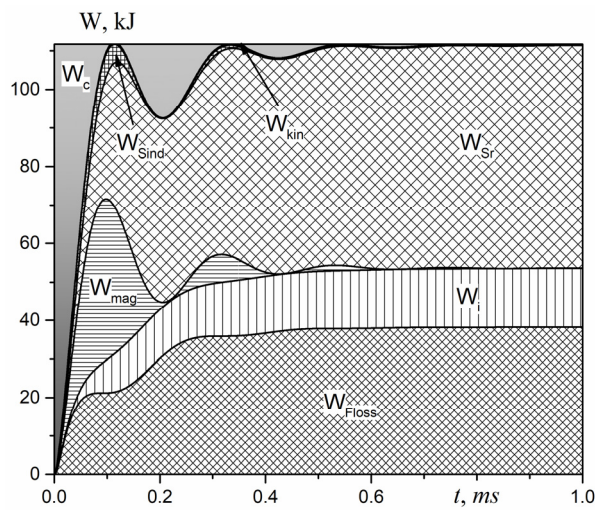


Fig. 4. Distribution of energy in the PIAPF

During the work process, the magnetic energy W_{mag} and the CES energy W_C have an oscillatory-damping character, and they change almost in antiphase. All other energy components in the accelerator grow to different levels, going to a certain constant value. As follows from the results of the calculation, the main part of the CES energy is transformed into thermal energy in the active elements and elements of the PIAPF excitation circuit.

Experimental studies of PIAPF. Experimental studies of the PIAPF of plasma formation were conducted on the basis of the Research and Design Institute «Molniya» using the methodology presented in [16]. The experimental setup includes the CES of the GITM-10/350 current generator, which consists of 120 parallel-connected IK503Y4 type capacitors, each of which has capacity of 3 μ F. The middle output of each capacitor is connected to the common bus through 4 TVO-60 resistors connected in parallel with resistance of 24 Ohms. Switching of CES is carried out through a high-voltage arrester.

Parameters of the experimental setup: the total capacity of the CES – 360 μ F, the maximum voltage of the CES – 50 kV, the measured active resistance of the inductor – 9 m Ω , the total resistance of the excitation circuit – 50 m Ω , the inductance of the inductor – 15 mH.

Experimental studies of the PIAPF with armature of various shapes and materials, made of conductive foil, were carried out. During the research, the inductor was horizontally attached to the insulating base, and an armature was installed on top of it through the insulating plate. This design of the accelerator ensured vertical movement of the armature under the action of electrodynamic forces.

The inductor was made in the form of a flat disc spiral made of steel with outer diameter of 600 mm. A gap is made between turns of the spiral, which ensures the impossibility of inter-turn electrical breakdown. The turns of the spiral are attached to the insulating plate with the help of steel screws (Fig. 5). The cross-section of the spiral turn was $5 \times 25 = 125$ mm². Two variants of the inductor were used in the experiments. In the first version

(7 turns), the inner turn of the inductor was placed in the center and the inductance of the inductor $L_1 = 12 \mu\text{H}$. In the second version, the two inner turns of the inductor were removed and the diameter of the inner hole was 230 mm.



Fig. 5. External view of the PIAPF inductor: the first version (a), the second version (b)

Figure 6 shows the results of the operation of the PIAPF, in which the armature is made as an aluminum foil with thickness of $18 \mu\text{m}$ in the form of a disc with outer diameter $D_{ex} = 600 \text{ mm}$ (Fig. 6,a), and the inductor of the first variant is connected to the CES with voltage $U_0 = 20 \text{ kV}$. After the tests, the disk armature is aluminum foil compressed into a volumetric wad (Fig. 6,b). During the operation of the accelerator, the armature enters the plasma state and moves vertically upwards for several meters (in Fig. 6,c,d, the armature is shown by a straight line).

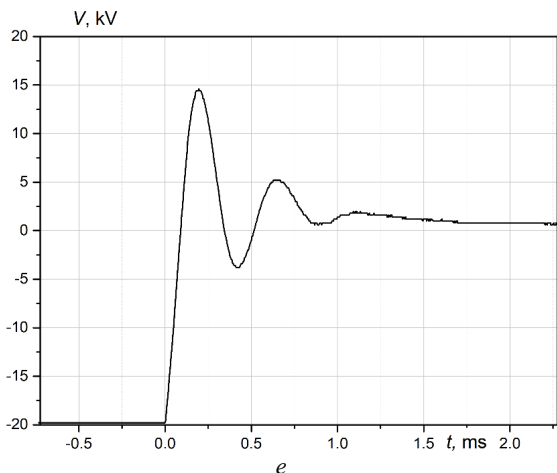
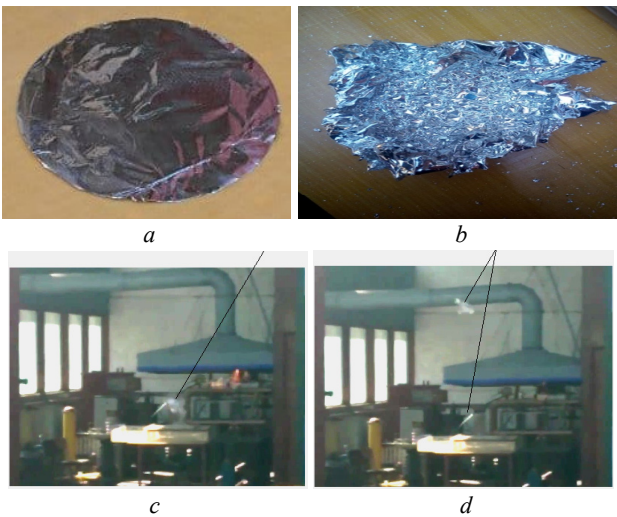


Fig. 6. Disk armature before (a) and after (b) tests, the position of the armature at the initial (c) and next (d) moments of operation and the oscillogram of the CES voltage (e) of the PIAPF

Figure 7 shows the results of the PIAPF operation, in which the armature is made in the form of a torus of aluminum foil with thickness of $10 \mu\text{m}$, and the inductor of the second variant is connected to the CES with voltage $U_0 = 23 \text{ kV}$. The average diameter of the torus is 300 mm (Fig. 7,a). When the accelerator was working, the toroidal armature, after transitioning into the plasma state, turned into a cluster of small particles that rose to a considerable height relative to the inductor (Fig. 7,b). The transformation of the armature, made of thinner foil than in the previous experiment, into a cluster of small particles can be explained both by the action of electrodynamic forces in the armature and by nonuniform thermal damage to its individual sections.

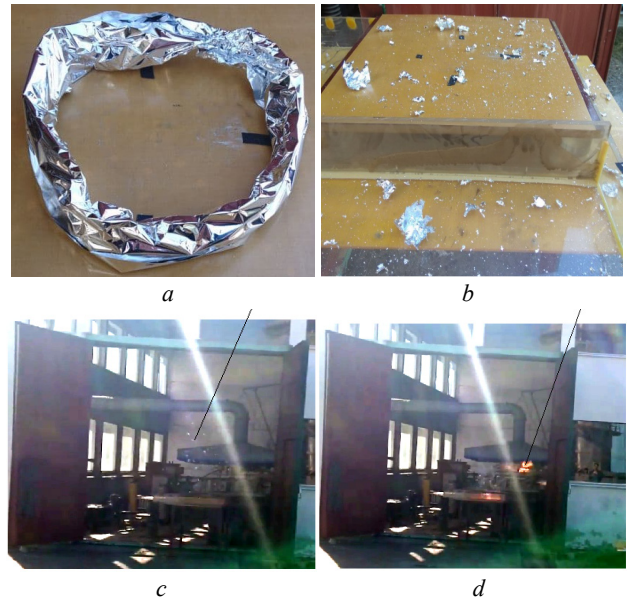


Fig. 7. Toroidal armature before (a) and after (b) tests; position of the armature at the initial (c) and next (d) moments of the PIAPF operation

Figure 8 shows the results of the PIAPF operation, in which the inductor of the second variant is excited at voltage $U_0 = 20 \text{ kV}$, and the armature is made of copper foil, 9 mm thick, which is fixed on a sheet of fiberglass with dimensions of $900 \times 900 \times 1 \text{ mm}$. Since the fiberglass sheet was curved, an insulating support with a load was used to press it evenly to the inductor (Fig. 8,a).

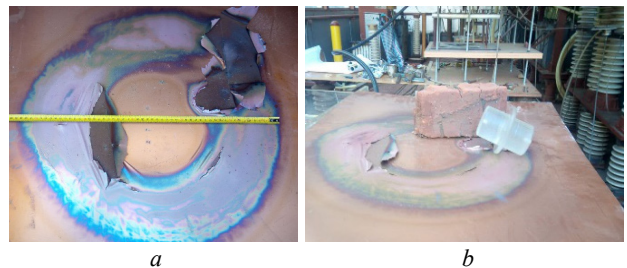


Fig. 8. Armature made of copper foil, which is fixed on a sheet from fiberglass, after PIAPF tests

After the operation of the accelerator, an area of thermal combustion (Fig. 8,b) appeared in the place where the glass-textolite sheet was pressed against the copper foil, the particles of which flew up. Here, the characteristic circular contour of the heating of the copper

foil is clearly visible, which indicates the similar nature of the induced current in the armature. Since the melting temperature of copper is higher than that of aluminum, thermal ionization of the copper foil did not occur even in the zone of induced current flow. In other areas, thermal heating of the foil is practically absent.

When using a more compact inductor (outer diameter 280 mm, coil width 9.4 mm, distance between coils 5 mm) on CES with higher voltage $U_0 = 35$ kV and with smaller capacity $C_0 = 18.5$ μ F (total resistance of the excitation circuit $R_0 = 0.1$ Ω , total inductance of the excitation circuit $L_0 = 1.5$ μ H) a plasma formation is formed, which moves relative to the inductor. Figure 9 shows an oscillogram of the current in the inductor, the external view of the inductor and the plasma formation that has moved away from the inductor. The armature is made of copper foil, 9 mm thick, which is fixed on a fiberglass sheet with dimensions of 900×900×1 mm.

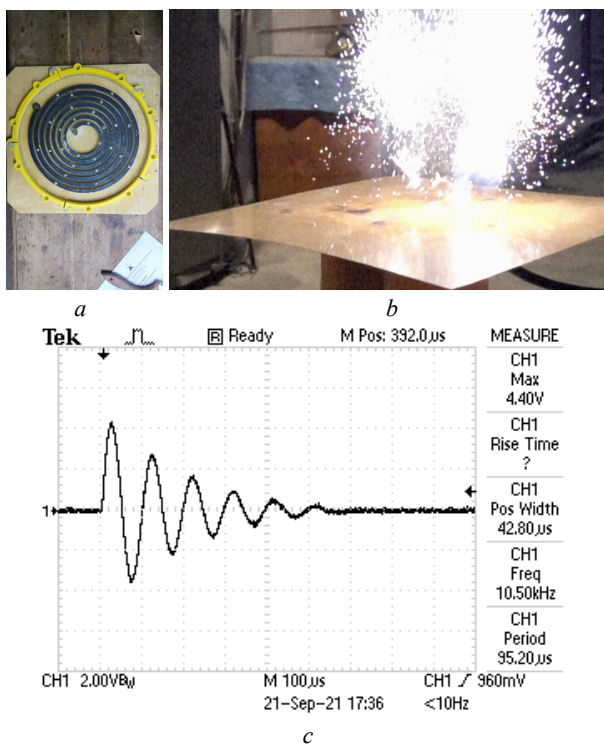


Fig. 9. External view of the inductor (a), the plasma formation (b) of the accelerator, and the oscillogram of the inductor current (c)

The oscillogram of the inductor current has an oscillatory-damping character with amplitude of the first half-wave of 51.6 kA. In Fig. 9,b, it can be seen that the plasma formation under the action of electrodynamic forces detaches from the sheet of copper foil and moves several meters vertically upwards.

Thus, if the CES voltage does not exceed certain values, then the induced current in the armature is relatively small and during the heating process does not form a thermally ionized plasma formation of a certain part of the copper foil. And with an increase in the CES voltage, there is an increase in the induced current in the armature, which carries out thermal ionization of the corresponding part of the armature with the transition into a plasma formation, which, under the action of electrodynamic forces, moves vertically upwards for several meters.

The results of experimental studies, namely, the shape, voltage and current in the inductor coincide with the calculated ones with accuracy of up to 15 %, which indicates the reliability of the mathematical model of the accelerator.

Thus, experimental and theoretical studies show the validity of the concept of a pulse induction accelerator, in which, due to the high density of the induced current in the armature made of electrically conductive foil, thermal ionization occurs as a result of an electric explosion of the conductor with its transition into a plasma state. The interaction of this plasma formation with the magnetic field of the inductor leads to the appearance of the electrodynamic force, which ensures its movement in the open atmospheric environment by several meters relative to the stationary inductor.

Conclusions.

1. Work on the creation and throwing of plasma formations is relevant and is carried out in leading scientific centers of the world using gas-dynamic and electromagnetic forces.

2. A mathematical model of a pulse induction accelerator was developed and implemented in the Comsol Multiphysics software package, in which the armature does not change its shape and aggregate state during operation. The mathematical model, which takes into account the parameters of the accelerator distributed in space, uses a system of partial differential equations with respect to spatial and temporal variables.

3. Electromechanical and thermal characteristics of the accelerator have been calculated. It is shown that the temperature rise in the aluminum foil armature is significantly nonuniform. The maximum temperature value occurs in the middle part of the foil closer to the outer edge, and this temperature significantly exceeds the boiling point of aluminum.

4. Experimental research was carried out on an accelerator in which the armature is made of aluminum and copper foil, and the inductor connected to the high-voltage CES is made of steel in the form of a flat disk spiral. It was established that during the operation of the accelerator, the armature enters a plasma state and moves vertically upwards for several meters, turning into a volumetric wad or a cluster of small particles that rose to a considerable height relative to the inductor.

5. The characteristic circular contour of the thermal heating of the copper foil of the armature, which is fixed on a glass-textolite sheet, is experimentally shown, which indicates a similar nature of plasma formation.

Conflict of interest. The authors of the article declare that there is no conflict of interest.

REFERENCES

1. Myers C.E., Belova E.V., Brown M.R., Gray T., Cothran C.D., Schaffer M.J. Three-dimensional magnetohydrodynamics simulations of counter-helicity spheromak merging in the Swarthmore Spheromak Experiment. *Physics of Plasmas*, 2011, vol. 18, no. 11, pp. 112512-112530. doi: <https://doi.org/10.1063/1.3660533>.
2. Gray T., Lukin V.S., Brown M.R., Cothran C.D. Three-dimensional reconnection and relaxation of merging spheromak plasmas. *Physics of Plasmas*, 2010, vol. 17, no. 10, pp. 102106-102114. doi: <https://doi.org/10.1063/1.3492726>.

3. Ji H., Daughton W. Phase diagram for magnetic reconnection in heliophysical, astrophysical, and laboratory plasmas. *Physics of Plasmas*, 2011, vol. 18, no. 11, pp. 111207-111217. doi: <https://doi.org/10.1063/1.3647505>.
4. Baalrud S.D., Bhattacharjee A., Huang Y.-M., Germaschewski K. Hall magnetohydrodynamic reconnection in the plasmoid unstable regime. *Physics of Plasmas*, 2011, vol. 18, no. 9, pp. 092108-092116. doi: <https://doi.org/10.1063/1.3633473>.
5. Sebastian Anthony. *Open-air plasma device could revolutionize energy generation, US Navy's weaponry*. Available: <https://www.extremetech.com/defense/153630-open-air-plasma-device-could-revolutionize-energy-generation-us-navys-weaponry> (accessed 10.05.2022).
6. Curry R.D. *Systems and Methods to Generate a Self-Confined High Density Air Plasma*. Patent US WO2012173864. 2012. Available: <https://patentscope.wipo.int/search/en/detail.jsf?docId=WO2012173864>. (accessed 10.01.2023).
7. Takahashi K. Helicon-type radiofrequency plasma thrusters and magnetic plasma nozzles. *Reviews of Modern Plasma Physics*, 2019, vol. 3, no. 1, art. no. 3. doi: <https://doi.org/10.1007/s41614-019-0024-2>.
8. Shumeiko A.I., Telekh V.D., Mayorova V.I. Development of a novel wave plasma propulsion module with six-directional thrust vectoring capability. *Acta Astronautica*, 2022, vol. 191, pp. 431-437. doi: <https://doi.org/10.1016/j.actaastro.2021.11.028>.
9. Guo J. Induction plasma synthesis of nanomaterials. *Plasma Science and Technology – Progress in Physical States and Chemical Reactions*. Rijeka, InTech, 2016. pp. 3-30. doi: <https://doi.org/10.5772/62549>.
10. Rudikov A.I., Antropov N.N., Popov G.A. Pulsed plasma thruster of the erosion type for a geostationary artificial Earth satellite. *Acta Astronautica*, 1995, vol. 35, no. 9–11, pp. 585-590. doi: [https://doi.org/10.1016/0094-5765\(95\)00025-U](https://doi.org/10.1016/0094-5765(95)00025-U).
11. Spanjers G., McFall K., Gulczinski III F., Spores R. Investigation of propellant inefficiencies in a pulsed plasma thruster. *32nd Joint Propulsion Conference and Exhibit*, 1996. doi: <https://doi.org/10.2514/6.1996-2723>.
12. Takahashi K. Magnetic nozzle radiofrequency plasma thruster approaching twenty percent thruster efficiency. *Scientific Reports*, 2021, vol. 11, no. 1, art. no. 2768. doi: <https://doi.org/10.1038/s41598-021-82471-2>.
13. Di Canto G. *Plasma propulsion system and method*. Patent US WO2016151609. 2016. Available: <https://patentscope.wipo.int/search/en/detail.jsf?docId=WO2016151609&cid=P10-LL70BV-97870-1>. (accessed 10.01.2023).
14. Polzin K.A., Choueiri E.Y. Performance optimization criteria for pulsed inductive plasma acceleration. *IEEE Transactions on Plasma Science*, 2006, vol. 34, no. 3, pp. 945-953. doi: <https://doi.org/10.1109/TPS.2006.875732>.
15. Korytchenko K.V., Bolyukh V.F., Rezinkin O.L., Burjakovskij S.G., Mesenko O.P. Axial coil accelerator of plasma ring in the atmospheric pressure air. *Problems of Atomic Science and Technology*, 2019, vol. 119, no. 1, pp. 120-123.
16. Bolyukh V.F., Kocherga A.I. Efficiency and Practical Implementation of the Double Armature Linear Pulse Electromechanical Accelerator. *2021 IEEE 2nd KhPI Week on Advanced Technology (KhPIWeek)*, 2021, pp. 153-158. doi: <https://doi.org/10.1109/KhPIWeek53812.2021.9570065>.
17. Bolyukh V.F., Schukin I.S. Excitation with a series of pulses of a linear pulse electrodynamic type converter operating in power and high-speed modes. *Electrical Engineering & Electromechanics*, 2020, no. 4, pp. 3-11. doi: <https://doi.org/10.20998/2074-272X.2020.4.01>.

Received 08.01.2023
Accepted 15.03.2023
Published 01.09.2023

K.V. Korytchenko¹, Doctor of Technical Science, Professor,
V.F. Bolyukh¹, Doctor of Technical Science, Professor,
S.G. Buriakovskiy², Doctor of Technical Science, Professor,
Y.V. Kashansky¹,
O.I. Kocherga¹, PhD,
¹National Technical University «Kharkiv Polytechnic Institute»,
2, Kyrpychova Str., Kharkiv, 61002, Ukraine,
e-mail: korytchenko_kv@ukr.net;
vfbolyukh@gmail.com (Corresponding Author);
yurii.kashanskyi@khpi.edu.ua;
kocherga.oleksandr07@gmail.com
²Research and Design Institute «Molniya»
of National Technical University «Kharkiv Polytechnic Institute»,
47, Shevchenko Str., Kharkiv, 61013, Ukraine,
e-mail: sergbyr@i.ua

How to cite this article:

Korytchenko K.V., Bolyukh V.F., Buriakovskiy S.G., Kashansky Y.V., Kocherga O.I. Electromechanical and thermophysical processes in the pulse induction accelerator of plasma formation. *Electrical Engineering & Electromechanics*, 2023, no. 5, pp. 69-76. doi: <https://doi.org/10.20998/2074-272X.2023.5.10>